Available online at www.sciencedirect.com
SCIENCE DIRECT®
ELSEVIER
International Journal of Solids and Structures 42 (2005) 3375–3394
INTERNATIONAL JOURNAL OF SOLIDS and STRUCTURES
www.elsevier.com/locate/ijsolstr

Multiple slip in a strain-gradient plasticity model motivated by a statistical-mechanics description of dislocations

S. Yefimov [1], E. Van der Giessen *

Netherlands Institute for Metals Research/Department of Applied Physics, University of Groningen, Nyenborgh 4, 9747 AG Groningen, The Netherlands

Received 11 June 2004; received in revised form 20 October 2004
Available online 10 December 2004

Abstract

We have recently proposed a nonlocal continuum crystal plasticity theory for single slip, which is based on a statistical-mechanics description of the collective behavior of dislocations in two dimensions. In the present paper we address the extension of the theory from single slip to multiple slip. Continuum dislocation dynamics in multiple slip is defined and coupled to the small-strain framework of conventional continuum crystal plasticity. Dislocation nucleation, the material resistance to dislocation glide and dislocation annihilation are included in the formulation. Various nonlocal interaction laws between different slip systems are considered on phenomenological grounds. To validate the theory we compare with the results of dislocation simulations of two boundary value problems. One problem is simple shearing of a crystalline strip constrained between two rigid and impenetrable walls. Key features are the formation of boundary layers and the size dependence of the response in the case of symmetric double slip. The other problem is bending of a single crystal strip under double slip. The bending moment versus rotation angle and the evolution of the dislocation structure are analyzed for different slip orientations and specimen sizes.

Keywords: Constitutive behavior; Crystal plasticity; Dislocations; Finite elements

1. Introduction

There is a growing body of experimental evidence that anisotropic plastic flow in crystalline solids is inherently size dependent at length scales of the order of tens of micrometers and smaller. Size effects of

* Corresponding author.
E-mail address: giessen@phys.rug.nl (E. Van der Giessen).
[1] Present address: Department of Chemistry, University of Groningen, Nyenborgh 4, 9747 AG Groningen, The Netherlands.

0020-7683/$ - see front matter © 2004 Elsevier Ltd. All rights reserved.
doi:10.1016/j.ijsolstr.2004.10.025

the type "smaller is stronger" are common at these scales and have been observed, for example, by Fleck et al. (1994) in torsion, and by Ma and Clarke (1995) and by Stölken and Evans (1998) in composites and in bending, respectively.

Standard continuum crystal plasticity models are local and do not make reference to the microstructural characteristic lengths that are significant at these scales. As a consequence, such models exhibit no size dependence. This creates a motivation to develop more sophisticated (nonlocal) models that incorporate such a length scale and, therefore, should be able to capture size effects (Hutchinson, 2000). However, there is no unified structure of such nonlocal theories. Therefore, there are a number of nonlocal (or strain-gradient) crystal plasticity theories available in the literature which introduce nonlocality in different ways. A subset of them is based on the idea that the geometrically necessary dislocations associated with strain gradients give rise to additional hardening. Most of these employ Nye's (1953) geometrical concept of a dislocation density tensor, but in a variety of ways. Irrespective of the precise formulation, a constant material length scale enters in such theories which needs to be fitted to experimental results (see, e.g., Fleck et al. (1994), Fleck and Hutchinson (1997) and Gao et al. (1999)) or to results of discrete dislocation simulations, e.g. Bassani et al. (2001); Shu et al. (2001); Bittencourt et al. (2003).

While the above-referenced approaches are completely phenomenological, this paper is concerned with an alternative approach: a recently proposed nonlocal crystal plasticity theory (Yefimov et al., 2004a) that augments a standard crystal plasticity description with a statistical-mechanics description of the collective behavior of dislocations in two dimensions (Groma, 1997). Initially, the theory was proposed in single slip (Yefimov et al., 2004a). Starting out from a statistical-mechanics treatment of an ensemble of gliding dislocations, the resulting dislocation dynamics is governed by two coupled balance equations for the total dislocation density and net-Burgers vector density. The latter can be interpreted as the density of geometrically necessary dislocations (GNDs).

To assess the validity of the approach, it has been applied to two boundary value problems. First we have analyzed shearing of a model composite material having elastic reinforcing particles (Yefimov et al., 2004a), while the other problem concerned bending of a single-crystal strip (Yefimov et al., 2004b). The nonlocal plasticity results were compared with those of discrete dislocation simulations of the same problems. The comparisons for the two problems have revealed the ability of the theory in single slip to capture the nonlocal effects and to treat the boundary value problems with physically different of boundary conditions.

The goal of the present study is to extend the theory from single slip to multiple slip. The key in multiple slip is the interaction between dislocations on different slip systems. By lack of a better procedure, several phenomenological interaction rules are proposed. They are evaluated first by analyzing the simple shearing of a crystal with two slip systems between two rigid and impenetrable walls. The results are compared with those of a discrete dislocation study by Shu et al. (2001) of the same problem, with emphasis on the formation of boundary layers and the associated size effects. One of the interaction laws is adopted subsequently in the study of bending of a single-crystal strip. We will show how the theory can handle this problem in symmetric double slip and will also discuss the correspondence with results of discrete dislocation simulations (Cleveringa et al., 1999).

2. Nonlocal continuum plasticity

The nonlocal continuum crystal plasticity formulation adopted here is based on the single-slip theory proposed by Yefimov et al. (2004a). The theory involves a statistical-mechanics description of the collective behavior of dislocations in two dimensions, which is coupled to standard single crystal continuum slip description. In this section we first give a brief summary of the theory for single slip and then proceed with an extension to multiple slip.

2.1. Summary of the theory for single slip

Starting out from the equation of motion of individual edge dislocations with Burgers vector $\boldsymbol{b}$ and applying a statistical averaging procedure, Groma (1997) has derived a continuum dynamics for dislocation densities in two dimensions. It involves the following set of coupled transport equations for the total dislocation density field $\rho = \rho_+ + \rho_-$ and for the net-Burgers vector density field $k = \rho_+ - \rho_-$:

$$\frac{\partial \rho}{\partial t} + \frac{\partial}{\partial \boldsymbol{r}} \cdot (k\boldsymbol{v}) = f(\rho, k, \ldots), \tag{1}$$

$$\frac{\partial k}{\partial t} + \frac{\partial}{\partial \boldsymbol{r}} \cdot (\rho\boldsymbol{v}) = 0, \tag{2}$$

where $\rho_\pm$ are the densities of the dislocations with Burgers vector $\pm\boldsymbol{b}$. $\boldsymbol{v}$ is the continuum dislocation glide velocity, defined as

$$\boldsymbol{v} = B^{-1}\boldsymbol{b}(\tau - \tau_s), \tag{3}$$

with $\tau = \boldsymbol{m} \cdot \boldsymbol{\sigma} \cdot \boldsymbol{s}$ being the resolved shear stress on the slip system defined by the unit vectors $\boldsymbol{s} = \boldsymbol{b}/|\boldsymbol{b}|$of the slip direction and the slip plane normal $\boldsymbol{m}$; $\boldsymbol{\sigma}$ is the stress tensor. The back stress τ_s in (3) arises from the gradient of the net-Burgers vector density along the slip direction as

$$\tau_s(\boldsymbol{r}) = \frac{\mu \boldsymbol{b}}{2\pi(1-\nu)\rho(\boldsymbol{r})} \cdot D\frac{\partial k}{\partial \boldsymbol{r}}. \tag{4}$$

Here, μ and ν are shear modulus and Poisson's ratio, respectively, and B is the dislocation drag coefficient. D is a dimensionless constant. It is noted that Gurtin's (2002) theory also involves a back stress that is determined by the gradient of net-Burgers vector, but it involves a material length scale as a new material constant; here the length scale is set by the local dislocation density, which evolves with deformation.

The function f in the right-hand side of (1) governs the rate of production of dislocations and is taken to have the form

$$f(\rho, k, \ldots) = C\rho_{\text{nuc}} \mid \tau - \tau_s \mid - AL_e(\rho + k)(\rho - k) \mid \boldsymbol{v} \mid . \tag{5}$$

The first term in the right-hand side represents nucleation from sources with a density ρ_{nuc} and at a rate governed by the parameter C given by

$$C = \frac{1}{\tau_{\text{nuc}} t_{\text{nuc}}} \quad \text{if} \quad \mid \tau - \tau_s \mid \geqslant \tau_{\text{nuc}}; \quad C = 0 \text{ otherwise}, \tag{6}$$

in terms of the nucleation strength τ_{nuc} and the nucleation time t_{nuc}. The second term in the right-hand side of (5) describes the annihilation of dislocations at a rate determined by $A|\boldsymbol{v}|$, with A being a dimensionless constant and L_e a material-dependent annihilation distance. Details can be found in Yefimov et al. (2004a).

The above continuum dislocation kinetics is coupled to the small-strain framework of single crystal continuum plasticity (see, e.g., Asaro, 1983). In summary, the plastic part $\dot{\boldsymbol{\varepsilon}}^{\text{p}}$ of the strain rate,

$$\dot{\boldsymbol{\varepsilon}} = \dot{\boldsymbol{\varepsilon}}^{\text{e}} + \dot{\boldsymbol{\varepsilon}}^{\text{p}}, \tag{7}$$

is expressed in terms of the slip rate $\dot{\gamma}$ on the slip system as

$$\dot{\boldsymbol{\varepsilon}}^{\text{p}} = \frac{1}{2}\dot{\gamma}(\boldsymbol{s} \otimes \boldsymbol{m} + \boldsymbol{m} \otimes \boldsymbol{s}), \tag{8}$$

and with $\dot{\gamma}$ linked to the average continuum dislocation glide velocity as $\dot{\gamma} = \rho\boldsymbol{b} \cdot \boldsymbol{v}$. Elasticity is specified by Hooke's law in the conventional form

$$\dot{\boldsymbol{\varepsilon}}^{\mathrm{e}} = \mathscr{L}^{-1}\dot{\boldsymbol{\sigma}}, \tag{9}$$

with $\mathscr{L}$ the tensor of elastic moduli.

In Yefimov et al. (2004a) we have also introduced the additional (and completely phenomenological) notion that the response of the material be elastic, i.e. $\dot{\gamma} = 0$, when

$$| \tau - \tau_s | < \tau_{\mathrm{res}}, \tag{10}$$

where τ_{res} is the slip resistance.

2.2. Extension to multiple slip

Let us consider a planar single crystal having $N \geqslant 1$ active slip systems, identified by Greek superscripts (no summation convention). Each slip system α ($\alpha = 1,\ldots,N$) is defined by a pair of the unit vectors $(\boldsymbol{s}^{(\alpha)}, \boldsymbol{m}^{(\alpha)})$ in the direction of slip and the slip plane normal, respectively, and $\boldsymbol{s}^{(\alpha)} = \boldsymbol{b}^{(\alpha)}/|\boldsymbol{b}^{(\alpha)}|$.

To define a continuum dislocation dynamics in multiple slip, we apply the single slip dynamics, Eqs. (1) and (2), for each slip system individually as follows:

$$\frac{\partial \rho^{(\alpha)}}{\partial t} + \frac{\partial}{\partial \boldsymbol{r}} \cdot (k^{(\alpha)} \boldsymbol{v}^{(\alpha)}) = f^{(\alpha)}, \tag{11}$$

$$\frac{\partial k^{(\alpha)}}{\partial t} + \frac{\partial}{\partial \boldsymbol{r}} \cdot (\rho^{(\alpha)} \boldsymbol{v}^{(\alpha)}) = 0. \tag{12}$$

The velocity $\boldsymbol{v}^{(\alpha)}$ is defined as

$$\boldsymbol{v}^{(\alpha)} = B^{-1}\boldsymbol{b}^{(\alpha)}(\tau^{(\alpha)} - \tau_{\mathrm{tot}}^{(\alpha)}) \tag{13}$$

in terms of the resolved shear stress $\tau^{(\alpha)} = \boldsymbol{m}^{(\alpha)} \cdot \boldsymbol{\sigma} \cdot \boldsymbol{s}^{(\alpha)}$ and the total back stress $\tau_{\mathrm{tot}}^{(\alpha)}$ on the slip system α. The actual form of $\tau_{\mathrm{tot}}^{(\alpha)}$ will be discussed later.

The production term $f^{(\alpha)}$ in Eq. (11) is defined similar to that in (5) in single slip with τ_s being substituted by ${\tau_{\mathrm{tot}}}^{(\alpha)}$, i.e.

$$f^{(\alpha)} = C^{(\alpha)}\rho_{\mathrm{nuc}}^{(\alpha)} \mid \tau^{(\alpha)} - \tau_{\mathrm{tot}}^{(\alpha)} \mid - AL_e(\rho^{(\alpha)} + k^{(\alpha)})(\rho^{(\alpha)} - k^{(\alpha)}) \mid \boldsymbol{v}^{(\alpha)} \mid . \tag{14}$$

The nucleation parameter $C^{(\alpha)}$ is therefore defined by

$$C^{(\alpha)} = \frac{1}{\tau_{\mathrm{nuc}} t_{\mathrm{nuc}}} \text{ if } \mid \tau^{(\alpha)} - \tau_{\mathrm{tot}}^{(\alpha)} \mid \geqslant \tau_{\mathrm{nuc}}; \quad C^{(\alpha)} = 0 \text{ otherwise.} \tag{15}$$

The elastic–plastic threshold is also defined per slip system and now expressed as

$$\dot{\gamma}^{(\alpha)} = 0 \text{ if } \mid \tau^{(\alpha)} - \tau_{\mathrm{tot}}^{(\alpha)} \mid < \tau_{\mathrm{res}}. \tag{16}$$

The slip rate $\dot{\gamma}^{(\alpha)}$ is linked to the average continuum dislocation glide velocity $\boldsymbol{v}^{(\alpha)}$ from Eq. (13) according to $\dot{\gamma}^{(\alpha)} = \rho^{(\alpha)}\boldsymbol{b}^{(\alpha)} \cdot \boldsymbol{v}^{(\alpha)}$.

Zaiser et al. (2001) have proposed a proper statistical treatment of two-dimensional dislocation dynamics in multiple slip, as a generalization of Groma's (1997) single slip approach adopted here. That generalized model includes a full range of dislocation–dislocation interactions and requires higher-order dislocation densities to describe the higher-order pair correlations of the dislocations in case of multiple slip. Due to the natural complexity of such an approach and its current status, it is difficult to derive explicit expressions for the nonlocal interactions between different slip systems based only on single dislocation densities available in this study. Therefore, to define the nonlocal interactions between the dislocations of different slip systems expressed here by the total back stress, we will adopt here a purely phenomenological approach.

We assume the total back stress is defined as a superposition of the single slip measures of back stress of all available slip systems with orientation dependent weight factors. Thus, we can define $\tau_{\text{tot}}^{(\alpha)}$ as

$$\tau_{\text{tot}}^{(\alpha)} = \sum_{\beta=1}^{N} S^{(\alpha\beta)} \tau_s^{(\beta)}, \tag{17}$$

with $S^{(\alpha\beta)}$ being interpreted as a projection matrix and $\tau_s^{(\alpha)}$ is the back stress from single slip approximation, cf. Eq. (4),

$$\tau_s^{(\alpha)} = \frac{\mu \boldsymbol{b}^{(\alpha)}}{2\pi(1-\nu)\rho^{(\alpha)}} \cdot D \frac{\partial k^{(\alpha)}}{\partial \boldsymbol{r}}. \tag{18}$$

On the other hand, $\tau_{\text{tot}}^{(\alpha)}$ can be also interpreted as a resolved shear component of the total back stress tensor $\boldsymbol{\sigma}_{\text{tot}}$ (Harder, 1999; Zaiser et al., 2001),

$$\tau_{\text{tot}}^{(\alpha)} = \boldsymbol{m}^{(\alpha)} \cdot \boldsymbol{\sigma}_{\text{tot}} \cdot \boldsymbol{s}^{(\alpha)}. \tag{19}$$

Here, we distinguish between two possibilities of constructing the total back stress tensor. Substitution into (19) and taking into account (17) yields the associated form for the projection matrix $S^{(\alpha\beta)}$:

Version 1:

$$\boldsymbol{\sigma}_{\text{tot}} = \sum_{\alpha} \tau_s^{(\alpha)} [\boldsymbol{m}^{(\alpha)} \otimes \boldsymbol{s}^{(\alpha)}], \tag{20}$$

$$S^{(\alpha\beta)} = \boldsymbol{m}^{(\alpha)} \cdot (\boldsymbol{m}^{(\beta)} \otimes \boldsymbol{s}^{(\beta)}) \cdot \boldsymbol{s}^{(\alpha)} = (\boldsymbol{m}^{(\alpha)} \cdot \boldsymbol{m}^{(\beta)})(\boldsymbol{s}^{(\alpha)} \cdot \boldsymbol{s}^{(\beta)}); \tag{21}$$

Version 2:

$$\boldsymbol{\sigma}_{\text{tot}} = \sum_{\alpha} \tau_s^{(\alpha)} [\boldsymbol{s}^{(\alpha)} \otimes \boldsymbol{m}^{(\alpha)} + \boldsymbol{m}^{(\alpha)} \otimes \boldsymbol{s}^{(\alpha)}], \tag{22}$$

$$S^{(\alpha\beta)} = \boldsymbol{m}^{(\alpha)} \cdot (\boldsymbol{s}^{(\beta)} \otimes \boldsymbol{m}^{(\beta)} + \boldsymbol{m}^{(\beta)} \otimes \boldsymbol{s}^{(\beta)}) \cdot \boldsymbol{s}^{(\alpha)}. \tag{23}$$

The second of these is the symmetric version of the first. In addition, we consider a simple interaction rule that involves only the slip directions:

Version 3:

$$S^{(\alpha\beta)} = \boldsymbol{s}^{(\alpha)} \cdot \boldsymbol{s}^{(\beta)}, \tag{24}$$

which is similar to that used by Gurtin (2002) in his strain-gradient single crystal plasticity theory.

In all three proposed versions, $S^{(\alpha\beta)} = S^{(\beta\alpha)}$ and the diagonal components of $S^{(\alpha\beta)}$ are equal to unity, so that the back stress produced by a slip system α has the largest effect on that slip system itself and a smaller effect on the other slip systems.

As the total back stress $\tau_{\text{tot}}^{(\alpha)}$ is specified, the continuum dislocation dynamics in multiple slip, Eqs. (11)–(17), can be coupled to the same framework of single crystal continuum plasticity as follows. The plastic slip rate $\dot{\boldsymbol{\varepsilon}}^{\text{p}}$ is related to the slip rates $\dot{\gamma}^{(\alpha)}$ via

$$\dot{\boldsymbol{\varepsilon}}^{\text{p}} = \sum_{\alpha=1}^{N} \dot{\gamma}^{(\alpha)} \boldsymbol{P}^{(\alpha)}, \tag{25}$$

where $\boldsymbol{P}^{(\alpha)}$ is the Schmid orientation tensor given by

$$\boldsymbol{P}^{(\alpha)} = \frac{1}{2}(\boldsymbol{s}^{(\alpha)} \otimes \boldsymbol{m}^{(\alpha)} + \boldsymbol{m}^{(\alpha)} \otimes \boldsymbol{s}^{(\alpha)}). \tag{26}$$

The elastic strain rate remains being governed by Hooke's law, Eq. (9).

3. Sensitivity of nonlocal interaction laws for constrained simple shear

3.1. Problem formulation

The three interaction laws proposed above are benchmarked by considering the simple shearing of a crystalline strip constrained between two rigid and impenetrable walls, as illustrated in Fig. 1. This problem was analyzed originally by Shu et al. (2001) and compared to a strain gradient theory of Shu and Fleck (1999), while subsequently it has been used for comparison with Gurtin's (2002) theory by Bittencourt et al. (2003). The crystal is assumed to have two slip systems. The strip is taken to be infinitely long but periodic, so that only a region of width w needs to be analyzed with periodic boundary conditions at $x_1 = 0$ and $x_1 = w$. The boundary conditions at the top and bottom of the strip are

$$\begin{aligned} &u_1 = 0, \quad u_2 = 0 \quad \text{along} \quad x_2 = 0; \\ &u_1 = U(t) = H\dot{\Gamma}t, \quad u_2 = 0 \quad \text{along} \quad x_2 = H, \end{aligned} \tag{27}$$

where $\dot{\Gamma}$ is the prescribed shear rate, taken to be constant in time t. In case of a classical local plasticity theory, the solution to this simple shearing boundary value problem for a homogeneous material and for uniform initial conditions is such that the only nonvanishing strain component, ε_{12}, is spatially uniform.

This changes drastically however in discrete dislocation plasticity when it is assumed that the dislocations cannot penetrate the top and bottom boundaries. This analysis is carried out using the Van der Giessen and Needleman (1995) approach, which is discussed in detail in Shu et al. (2001). Within that framework, the dislocations are treated as line defects in a linear elastic continuum. The computation of the deformation history is carried out in an incremental manner. Each time step involves three main steps: (i) determining the forces on the dislocations, i.e. the Peach–Koehler force; (ii) determining the rate of change of the dislocation structure, which involves the motion of dislocations, the generation of new dislocations, their mutual annihilation, and their possible pinning at obstacles; and (iii) determining the

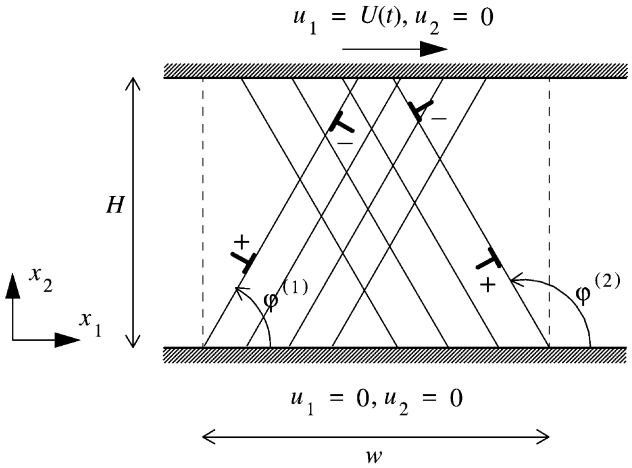

Fig. 1. Simple shear of a crystal with two slip systems between two impenetrable walls.

stress and strain state for the updated dislocation arrangement. The latter is obtained by superposition of the long-range singular fields for individual dislocations in infinite space and the image field that is calculated with the finite element method.

The numerical results for a strip with $H = 1\,\mu\text{m}$ (and cell width $w = 1\,\mu\text{m}$) subjected to a constant shear rate $\dot{\Gamma} = 10^3\,\text{s}^{-1}$ will serve as a reference for subsequent parameter studies. Two slip systems are considered, with the slip planes oriented at $\varphi^{(1)} = 60°$ and $\varphi^{(2)} = 120°$ from the x_1 axis. We will also analyze the effect of strip size by varying the height H of the strip and keeping the width w unchanged. In all cases, the material parameters of the crystal being used in the nonlocal continuum calculations are identical, whenever possible, to those of the discrete dislocation calculations of Shu et al. (2001), both for elastic and dislocation properties. The material is taken to be elastically isotropic, with shear modulus $\mu = 26.3\,\text{GPa}$ and Poisson ratio $\nu = 0.33$. The magnitude of the Burgers vector is $b = 0.25\,\text{nm}$ for all (edge) dislocations and a value $B = 10^{-4}\,\text{Pa s}$ for the drag coefficient is taken. These values are representative for aluminum.

In the analysis no dislocations are present initially and obstacles are not taken into account. In the discrete dislocation simulations new dislocations are generated in pairs from Frank–Read sources distributed in the material at a density $\rho_{\text{nuc}} = 138\,\mu\text{m}^{-2}$ for each slip system, when the resolved shear strength exceeds the source strength τ_{nuc} during a sufficiently long time $t_{\text{nuc}} = 10^{-8}$ s. The glide velocity $\boldsymbol{v}^{(I)}$ of dislocation I is linearly related to the Peach–Koehler force through the drag relation $\boldsymbol{F}^{(I)} = B\boldsymbol{v}^{(I)}$. Opposite-signed dislocations annihilate when they approach each other to within a distance of $L_e = 6b$.

Beside the material constants, the continuum theory has a few free parameters: the coefficient D in the back stress (4); the slip resistance τ_{res}, cf. Eq. (10); and the annihilation coefficient A in (5). Their values do not follow from the derivation of the transport equations and were fitted by Yefimov et al. (2004a) to discrete dislocation simulations for the problem of shearing of a two-dimensional composite material. The same values —$A = 5$, $D = 1$ and $\tau_{\text{res}} = 15$ MPa— are employed in this study. Hence, no further fitting is being done later in the paper.

Irrespective of the strip height, a uniform finite element mesh consisting of 30×30 quadrilateral elements is used to discretize the domain for both mechanical and dislocation dynamics subproblems. In the nonlocal continuum calculations the sources are distributed uniformly over all integration points in the matrix with a uniform density ρ_{nuc} per slip system. The strength of the dislocation sources is chosen randomly from a Gaussian distribution with mean value $\bar{\tau}_{\text{nuc}} = 1.9 \times 10^{-3}\,\mu$ and standard deviation $\Delta\tau_{\text{nuc}} = 0.2\bar{\tau}_{\text{nuc}}$ for both approaches.

Discretization of the nonlocal crystal plasticity equations is done by using the standard finite element method, and reported in detail in Yefimov et al. (2004a) for another boundary value problem. The dislocation dynamics part of the problem and the crystal plasticity part are decoupled by applying a staggered solution procedure for time integration. The solution of either of the two separate problems is obtained by using an explicit time-stepping scheme, with the same time steps for both subproblems.

Here, we pay attention only to the microscopic boundary conditions, required to solve the dislocation dynamics subproblem for this particular boundary value problem. Along the lateral sides $x_1 = 0$ and $x_1 = w$ of the unit cell, periodic boundary conditions are applied, so that $\rho^{(\alpha)}(w, x_2) = \rho^{(\alpha)}(0, x_2)$ and $k^{(\alpha)}(w, x_2) = k^{(\alpha)}(0, x_2)$ at all times. At the top and the bottom of the strip we model impenetrable walls for the dislocations. Thus, at these boundaries we require the dislocation velocity component normal to the boundary to vanish, i.e. $\mathbf{v}^{(\alpha)} \cdot \boldsymbol{n} = 0$, where $\boldsymbol{n}$ is the unit normal to the top and bottom surfaces.

3.2. Numerical results for the reference case

The overall material response is presented in terms of average shear stress, σ_{12}^{ave}, given by

$$\sigma_{12}^{\text{ave}} = \frac{1}{w}\int_0^w \sigma_{12}(x_1, H)\,\mathrm{d}x_1, \tag{28}$$

and its work-conjugate, the applied shear Γ.

The overall shear stress versus shear strain response using different nonlocal interaction laws is shown in Fig. 2. The shear stress σ_{12}^{ave} is normalized by the mean strength of the dislocation sources, $\bar{\tau}_{\text{nuc}} = 50\,\text{MPa}$. Fig. 2 shows that the material response is very sensitive to the nonlocal interaction law. In the continuum calculations the material exhibits a gradual transition to yield with nearly linear strain hardening at the largest strain levels. In the discrete dislocation simulations, despite the pronounced serrations due to individual dislocation events, a similar hardening tendency is observed. The hardening is related to the fact that the slip is blocked at the top and the bottom surfaces of the strip. Thus, the dislocations on the inclined slip planes pile-up against the surfaces and therefore produce a back stress on each activated slip system, which, in turn, significantly affects the overall response. This effect is picked up by the nonlocal theory as well, but depending upon the type of the applied nonlocal interactions, Eqs. (21), (23) or (24).

By comparing the nonlocal plasticity results with the discrete dislocation observation, it is seen that the best match is achieved by applying the interaction rule denoted as 'version 2', Eq. (23). The other interaction rules, including the uncoupled one, tend to overestimate the magnitude of the total back stress $\tau_{\text{tot}}^{(\alpha)}$, which, in turn, shifts the yield point upwards and gives rise to a higher hardening rate.

These observations confirm the conclusion in the discrete dislocation analysis by Shu et al. (2001) that the effective back stress on a slip system is smaller than the back stress from that individual slip system. The back stress that develops on one slip system is relaxed by the back stress produced by a dislocation structure of the other slip system. In the nonlocal continuum model the interaction rule (23) implies a similar behaviour due to compensating interactions arising from the negative off-diagonal elements of the projection matrix $S^{(\alpha\beta)}$ in Eq. (23). The other tested interaction rules give the opposite effect with $S^{(12)} = S^{(21)}$ being non-negative. *Thus, in the remainder of this paper we will use the nonlocal interaction rule from Eq. (23).*

The continuum dislocation distributions at $\Gamma = 0.015$ for slip system 1 oriented at $\varphi^{(1)} = 60°$ are shown in Figs. 3a and b in terms of the ρ and k fields, respectively. The corresponding plots for the second slip system ($\varphi^{(2)} = 120°$) are omitted here for brevity because they are similar. Qualitatively, Fig. 3 reveals the same dislocation structures as found in the discrete dislocation analysis of Shu et al. (2001), sampled in Fig. 4 at the same instant. Both approaches predict the formation of two distinct layers at the top

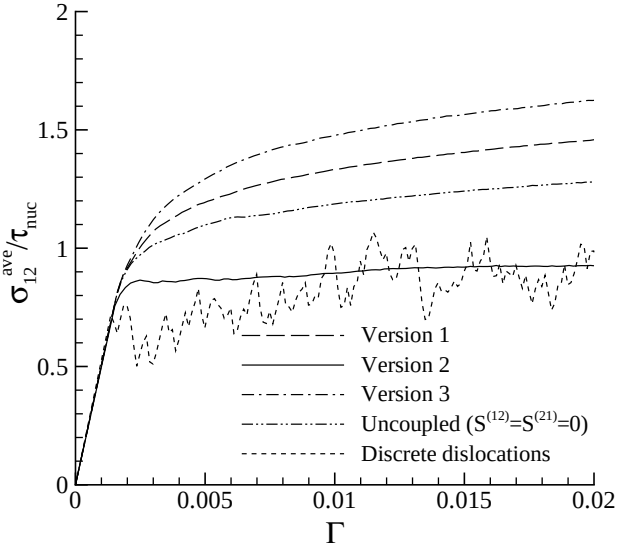

Fig. 2. Sensitivity of the average shear stress σ_{12}^{ave} versus applied shear strain Γ response to different slip systems interaction laws. Result of discrete dislocation plasticity is also shown.

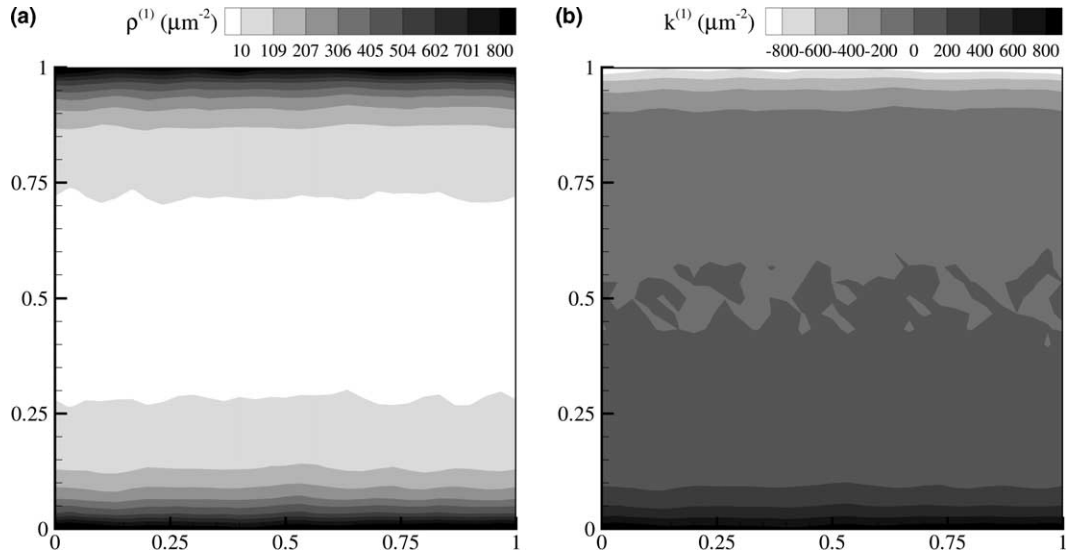

Fig. 3. Distributions of (a) the total dislocation density ρ and (b) the sign-dislocation density k at $\Gamma = 0.015$ for the slip system $\varphi^{(1)} = 60^\circ$ inside the unit cell for $H = 1\,\mu$m.

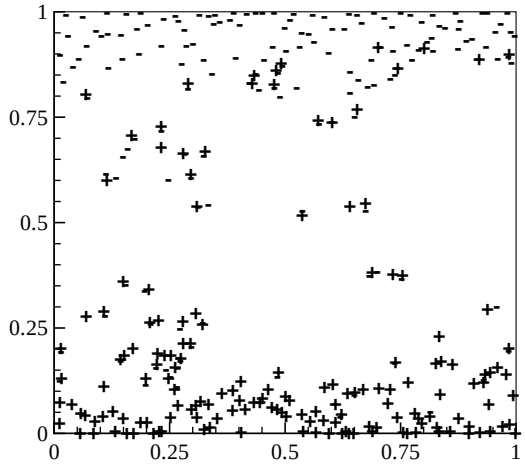

Fig. 4. Discrete dislocation distribution at $\Gamma = 0.015$ in the unit cell for $H = 1\,\mu$m. Positive dislocations are denoted by "+", negative ones by "−", cf. Fig. 1.

and bottom surfaces of the strip, densely populated by dislocations. The layers have been formed by the motion of like-signed dislocations (see Fig. 1 for the sign convention) that move from the core of the strip towards the surfaces. These so-called geometrically necessary dislocations (GNDs) pile-up against the top and bottom surfaces because of the imposed no-slip condition in the direction normal to the surfaces. The continuum plasticity calculations predict the thickness of each layer to be roughly 0.1–0.15 μm, which is consistent with the discrete dislocation observations (Shu et al., 2001).

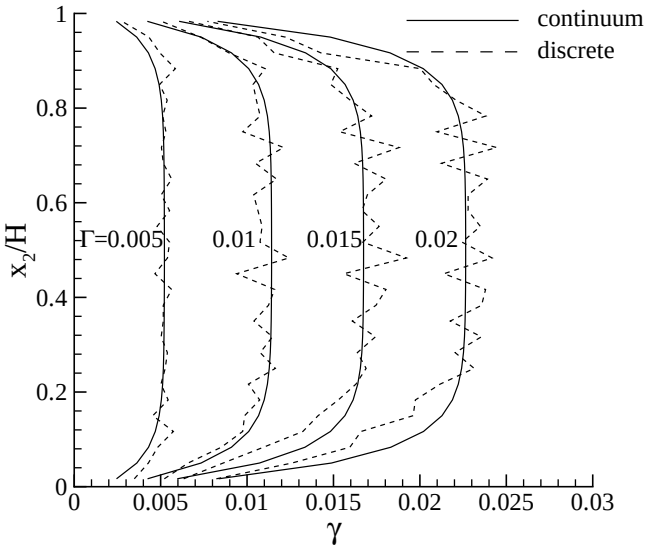

Fig. 5. Shear strain profiles across the strip height at various values of applied shear strain Γ for the strip with $H = 1\,\mu\text{m}$.

The formation of the boundary layers leads to a non-uniform spatial distribution of the shear strain component across the strip thickness. This is conveniently measured by the shear γ averaged over the x_1 direction, i.e.

$$\gamma(x_2) = \frac{2}{w}\int_0^w \varepsilon_{12}(x_1, x_2)\mathrm{d}x_1. \tag{29}$$

Fig. 5 shows the predictions of the γ distribution across the strip according to nonlocal continuum and discrete dislocation plasticity for the reference case. The results of the two approaches are in good agreement showing the systematic trend in boundary layer formation. The width of the boundary layers is increasing with ongoing deformation until around $\Gamma = 0.01$, and remains nearly constant afterwards. The width of the boundary layer in the strain profile at $\Gamma = 0.015$ is roughly the same as the thickness of the dislocation boundary layer seen in Figs. 3 and 4 at the same instant.

3.3. Size effects

In order to test the ability of the continuum theory to pick up size effects (Shu et al., 2001), we perform calculations for various strip heights H but otherwise identical parameters. Fig. 6 shows the effect of the strip height on the overall stress–strain response according to discrete dislocation and nonlocal continuum plasticity. The figure displays the systematic trend for the hardening rate as well as the flow strength to increase with decreasing strip height H. Evidently, the discrete dislocation results contain statistical effects, mostly on initial yield, through the distribution of source strengths; however, calculations for five different realizations of source strengths yield a spread of only 20% in the yield point. In the continuum plasticity calculations the size effect mainly appears in the initial flow strength, while the hardening rate dependence upon strip height is slightly less pronounced than that predicted in the discrete dislocation simulations. Nevertheless, beyond the elasticity–plasticity transition, the overall hardening for all sizes appears to be approximately linear with strain according and the tangent modulus $\mathrm{d}\sigma_{12}^{\mathrm{ave}}/\mathrm{d}\Gamma$ drops as the strip height increases.

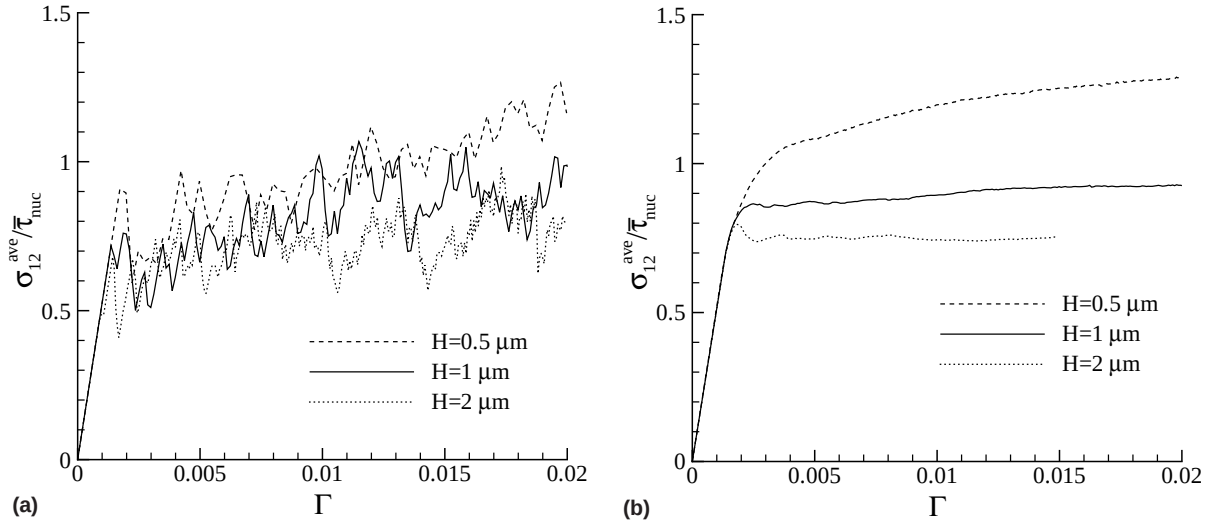

Fig. 6. Effect of strip height H on stress–strain response according to (a) discrete dislocation and (b) nonlocal continuum plasticity.

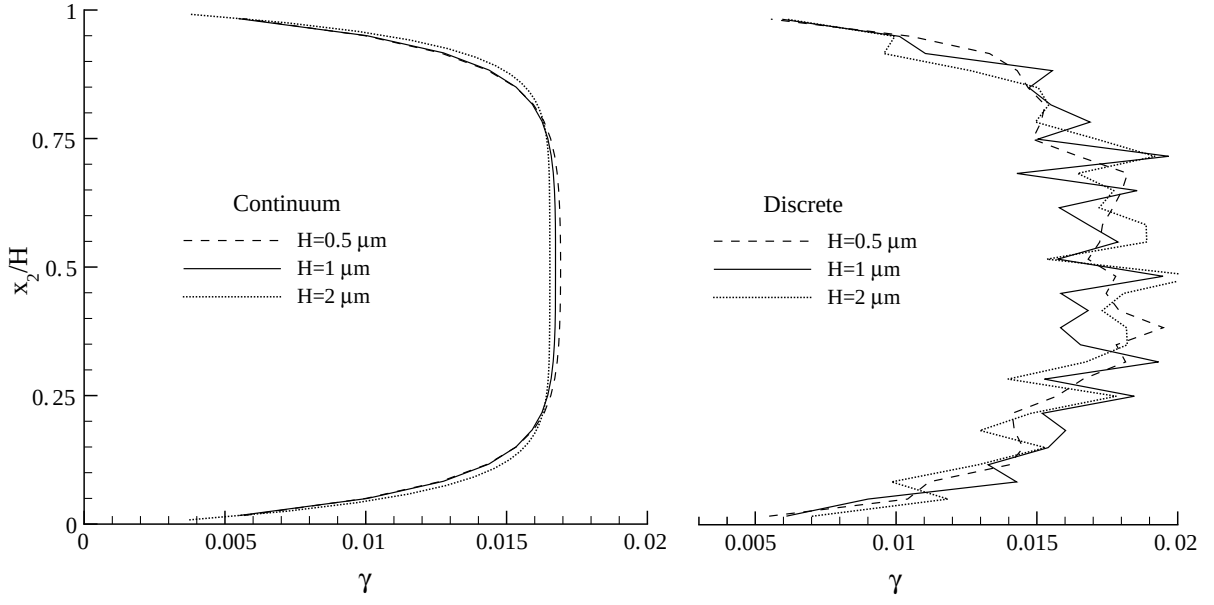

Fig. 7. Shear strain profiles at $\Gamma = 0.015$ for various strip heights H according to nonlocal continuum and discrete dislocation plasticity.

The size effect is triggered by the presence of the distinct boundary layers of GNDs through a delicate interplay between boundary layer thickness, internal strain gradient and plastic strain in the bulk. Fig. 7 demonstrates the effect of size on the strain distribution for various strip heights, by plotting $\gamma(x_2/H)$. If this field were identical for the different values of H, the boundary layer, as measured by this quantity,

would scale with the strip size; complete scaling with H would evidently imply size independence. The response is size dependent but the strain profile is not a very sensitive exponent of it.

4. Bending of a single crystal

The second benchmark problem to confront the nonlocal theory against discrete dislocation results is bending of a single crystal in double slip, as analyzed originally by Cleveringa et al. (1999). A strip of width L and height h is subjected to a rotation θ along its edges (see Fig. 8) through the boundary conditions

$$u_1(t) = \pm\theta x_2, \quad \sigma_{12} = 0 \quad \text{on } x_1 = \pm L/2, \tag{30}$$

with plane strain conditions normal to the x_1–x_2 plane. Traction-free boundary conditions are imposed along the top and bottom sides of the strip:

$$\sigma_{12} = \sigma_{22} = 0 \quad \text{on } x_2 = \pm h/2. \tag{31}$$

Slip by the motion of edge dislocations ($b = 0.25\,\text{nm}$) on two slip systems occurs inside the highlighted area of the strip in Fig. 8; this region is designed so that the lateral sides, where displacements are prescribed along $x_1 = \pm L/2$, always remain elastic.

Most of the results will be presented for a strip having dimensions $L = 12\,\mu\text{m}$ and $h = 4\,\mu\text{m}$ (the reference case), subjected to a bending rate of $\dot{\theta} = 10^3\ \text{s}^{-1}$. The strip has two slip systems, oriented at $\varphi^{(1)} = 30°$ and $\varphi^{(2)} = 150°$ from the x_1 axis. The plasticity parameters are the same, both elastically and plastically, as in the previous section and as in Yefimov et al. (2004b) where the same problem was addressed but in single slip.

No dislocations are presumed present initially, but Frank–Read sources are distributed in the material, having a mean strength $\bar{\tau}_{\text{nuc}} = 1.9 \times 10^{-3}\,\mu$ and standard deviation $\Delta\tau_{\text{nuc}} = 0.2\bar{\tau}_{\text{nuc}}$. For the reference case there are 202 sources that are evenly distributed and randomly positioned among 101 slip planes per slip system. This leads to an average source density $\rho_{\text{nuc}} = 10\,\mu\text{m}^{-2}$ (inside the plastic zone) for each slip system. In the continuum calculations the sources are distributed uniformly over all integration points in the matrix with a uniform density $\rho_{\text{nuc}}^{(\alpha)} = 10\ \mu\text{m}^{-2}$ for each of the two slip systems. The strength distribution of the sources is calculated separately for the two slip systems. The nucleation time is taken to be equal to $t_{\text{nuc}} = 10^{-8}$ s for all sources.

A uniform finite element mesh consisting of 66×38 quadrilateral elements is used to discretize the domain for both mechanical and dislocation dynamics subproblems. Numerical discretization of the model as well as treatment of the microscopic boundary conditions for the dislocation dynamics subproblem have been discussed in detail in Yefimov et al. (2004b).

The effect of strip size is studied by varying L and h such that the ratio h/L remains unchanged. The overall response will be presented in terms of the bending moment, M, calculated from the stress state by

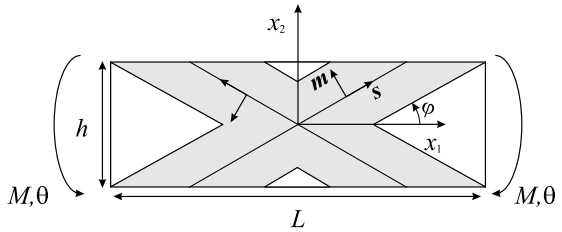

Fig. 8. Plastic bending of a two-dimensional strip with two symmetric slip systems.

$$M = \int_{-h/2}^{h/2} x_2 \sigma_{11}(\pm L/2, x_2) \mathrm{d}x_2. \tag{32}$$

The moment M is normalized by a reference moment

$$M_{\mathrm{ref}} = \frac{2}{h} \int_{-h/2}^{h/2} \bar{\tau}_{\mathrm{nuc}} x_2^2 \mathrm{d}x_2 = \frac{2}{3} \bar{\tau}_{\mathrm{nuc}} \left(\frac{h}{2}\right)^2, \tag{33}$$

that would result from the linear stress distribution $\bar{\tau}_{\mathrm{nuc}} x_2/(h/2)$.

The bending moment response to the imposed rotation according to both plasticity descriptions is shown in Fig. 9a for the reference case. The continuum plasticity result for the case with only one slip system at $\varphi^{(1)} = 30°$ is shown for comparison. The bending response for single slip is seen to be significantly harder than for double slip. In the latter case, a very low hardening rate (on average) is observed. The prediction of the continuum model for the total dislocation density evolution is also in good agreement with the discrete dislocation simulations.

The discrete dislocation distribution at $\theta = 0.015$ is shown in Fig. 10. Only few of the 101 available slip planes of each slip system have been activated. It is also seen that the two slip systems are, on average, equally populated with dislocations and that they are arranged mainly in well-defined pile-ups with dislocation-free areas near the top and bottom free surfaces. There are a few locations in the matrix, where some of the pile-ups of one slip system are blocked by dislocations on the other slip system. Slip becomes locally hindered there, the local stress from dislocations on one slip systems increases and can trigger dislocation generation on other slip systems. The dislocations being nucleated due to such process are "statistical" ones rather than the GNDs that are required to accommodate the applied deformation. This explains why the total dislocation density for double slip is higher than that in single slip (cf. Yefimov et al., 2004b).

The continuum dislocation distributions in terms of the ρ and k fields at $\theta = 0.015$ are shown in Figs. 11 and 12 for slip systems 1 and 2, respectively. Qualitatively, these fields have a similar structure as found

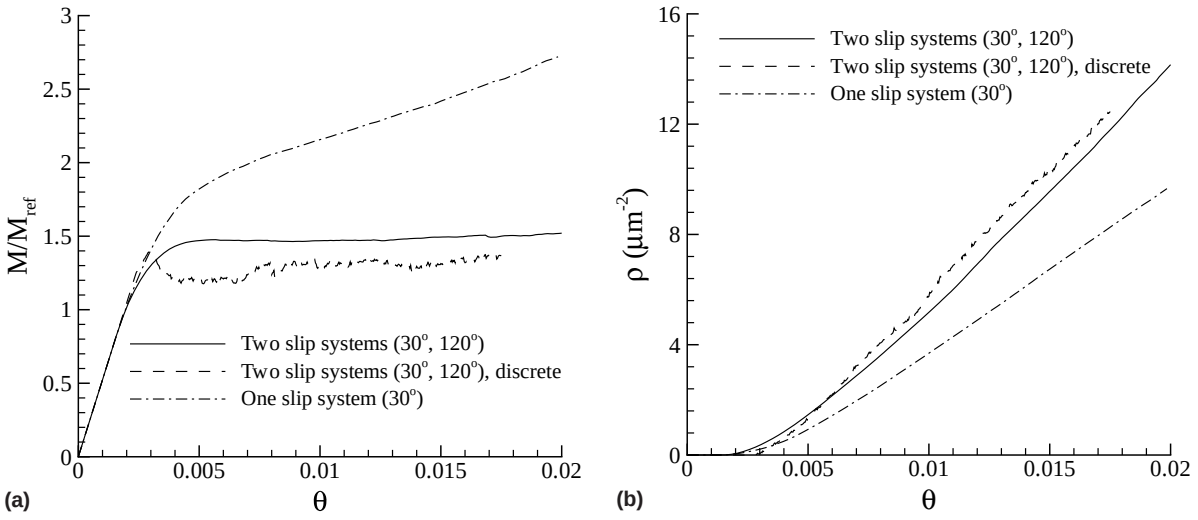

Fig. 9. Comparison of (a) bending response and (b) evolution of the accumulated total dislocation density $\rho = \rho^{(1)} + \rho^{(2)}$, for the reference case (30°, 150°) according to nonlocal continuum and discrete dislocation plasticity. Result for single slip case ($\varphi = 30°$) is also shown.

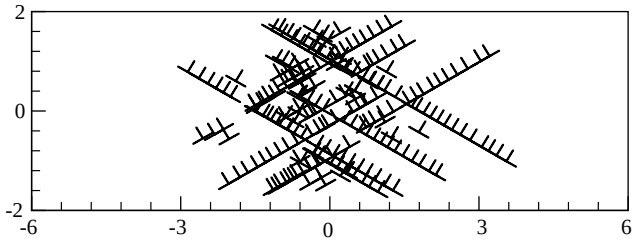

Fig. 10. Dislocation distribution at $\theta = 0.015$ for the reference case (30°, 150°).

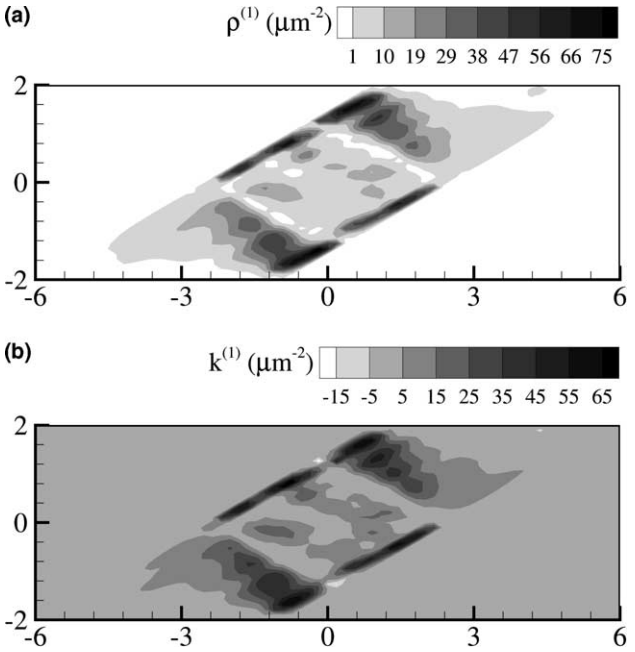

Fig. 11. Distributions of (a) the total dislocation density $\rho^{(1)}$ and (b) the sign-dislocation density $k^{(1)}$ at $\theta = 0.015$ on slip system 1 in the reference case (30°, 150°).

in the discrete dislocation analysis in Fig. 10. The levels of the total dislocation density, $\rho^{(1)}$, and the net-Burgers vector density, $k^{(1)}$, show that in slip system 1 ($\varphi^{(1)} = 30°$) the positive dislocations dominate, even though, for the reason described above, not all of them are GNDs. The second slip system ($\varphi^{(2)} = 150°$) reveals qualitatively similar behaviour, but with negative dislocations dominating. We also see that the continuum model predicts dislocation-free boundary layers near the free surfaces, much like the discrete simulations. This effect has been explained in detail by Yefimov et al. (2004b).

The development of the statistical dislocation population in the matrix can be observed in Fig. 13, where the evolution of the total dislocation density accumulated on the two slip systems is plotted versus plastic curvature. The plastic curvature is computed at each deformation stage as (Cleveringa et al., 1999)

$$\kappa^{\mathrm{p}} = \frac{2\theta}{L} - \frac{M}{EI}. \tag{34}$$

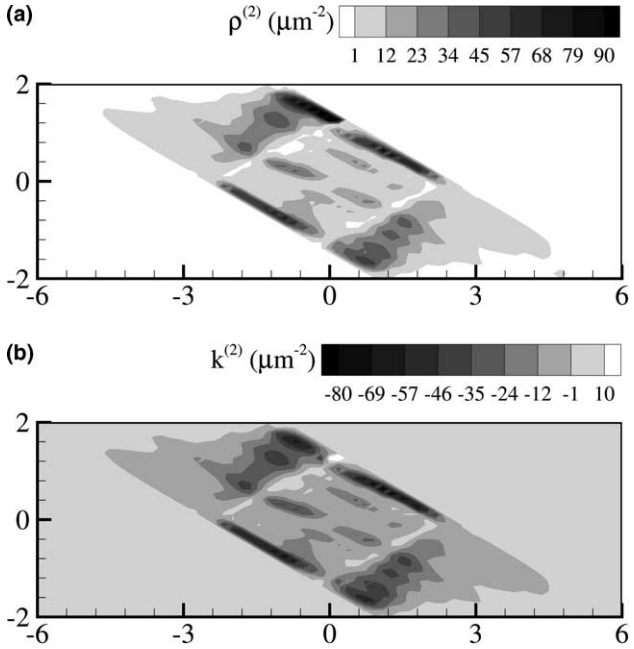

Fig. 12. Distributions of (a) the total dislocation density $\rho^{(2)}$ and (b) the sign-dislocation density $k^{(2)}$ at $\theta = 0.015$ on slip system 2 in the reference case (30°, 150°).

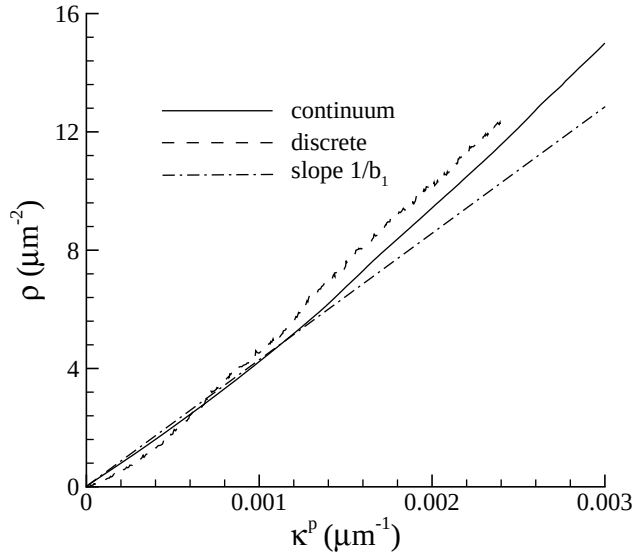

Fig. 13. Evolution of the total dislocation density $\rho = \rho^{(1)} + \rho^{(2)}$ versus plastic curvature for the reference case (30°, 150°) according to discrete and continuum plasticity.

The first term in the right-hand side is the total curvature and the second is the elastic curvature, where $EI = \mu h^3/6(1-\nu)$ is the bending stiffness in plane strain. According to Nye (1953) and Ashby (1970) the GND density for bending reads

$$\rho_G = \frac{\kappa^{\mathrm{p}}}{b_1}, \tag{35}$$

where $b_1 = b\cos\varphi$. Fig. 13 shows that the total dislocation density initially increases linearly with the plastic curvature κ^p with a slope slightly smaller than $1/b_1$, but from around $\kappa^p = 0.001$ the dislocation density increases faster than linear. The latter is attributed to a growing contribution of the statistical dislocations to the total dislocation density. Despite some quantitative deviation from the discrete dislocation result, the continuum model with the chosen rule for nonlocal interactions is capable of picking up this effect qualitatively correctly.

To study the effect of slip system orientation with the nonlocal continuum model, we repeat the calculation for a strip having two slip systems at $\varphi^{(1)} = 60°$ and $\varphi^{(2)} = 120°$. For this case we take the dislocation source density $\rho_{\mathrm{nuc}} = 17\,\mu\mathrm{m}^{-2}$ (inside the plastic zone for each slip system), which corresponds to 670 dislocation sources evenly distributed between the 335 slip planes per slip system in the discrete dislocation simulations. Comparison of results from discrete and continuum calculations in Fig. 14 reveals that the continuum model with the applied symmetric nonlocal interaction rule (23) is also able to predict the dependence of bending response on slip system orientation, as seen originally in dislocation simulations. Fig. 15a shows that the dislocation distribution for the $(60°, 120°)$ orientation is more uniform than in the reference case. The discrete dislocation simulations predict the formation of individual, regularly spaced slip bands, while the continuum model (Fig. 15b) gives rise to a dislocation-free zone near the neutral line ($y = 0$) and resolves a few individual slip bands near the elastic–plastic interface. As discussed for single slip by Yefimov et al. (2004b), the dislocation-free core originates from a non-zero value of τ_{res}.

Next we consider the effect of specimen size on the bending response. Fig. 16a compares the bending response for the reference $12\,\mu\mathrm{m} \times 4\,\mu\mathrm{m}$ specimen with that of a two times larger specimen ($24\,\mu\mathrm{m} \times 8\,\mu\mathrm{m}$)

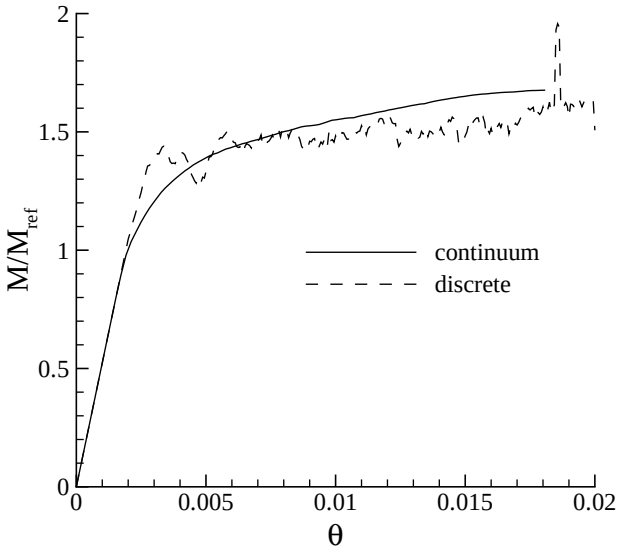

Fig. 14. Bending moment, M, versus imposed rotation, θ, curves for the case (60°, 120°) according to nonlocal continuum and discrete dislocation plasticity.

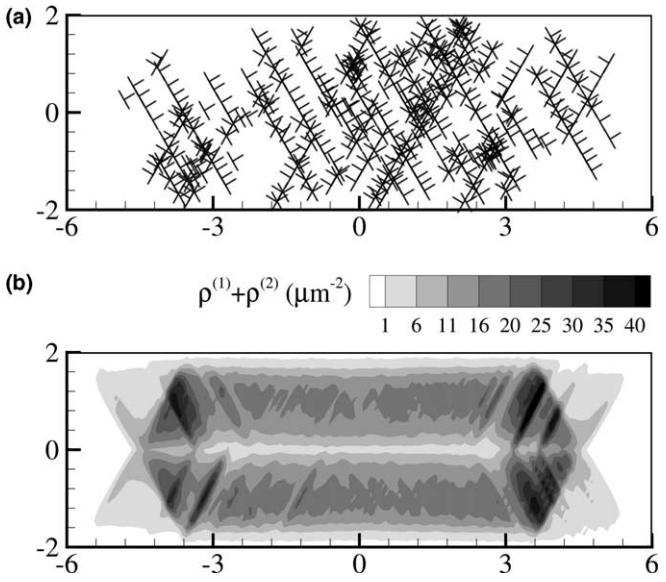

Fig. 15. Distribution of (a) dislocations according to discrete dislocation plasticity and (b) the accumulated total dislocation density $\rho^{(1)} + \rho^{(2)}$ of two slip systems 60° and 120° at $\theta = 0.015$.

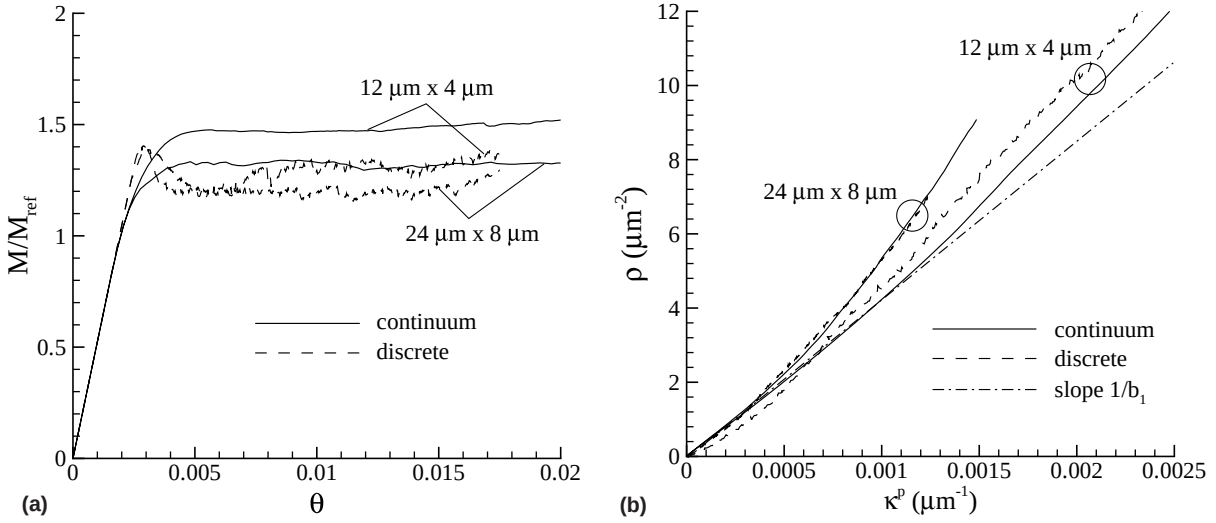

Fig. 16. Effect of specimen size for slip systems at (30°, 150°) on (a) the moment versus rotation angle and (b) total dislocation density evolution versus plastic curvature according to nonlocal continuum and discrete dislocation plasticity.

with two slip systems at $\varphi^{(1)} = 30°$ and $\varphi^{(2)} = 150°$. The bigger specimen has the same source density as defined in the reference case. In the continuum calculations the Gaussian distribution of source strength is the same for both specimens, as generated in the reference case. For the discrete dislocation simulations the random distributions of position and strength of the sources are generated independently for the two specimens, so that this by itself gives some statistical difference in the response in addition to the size effect.

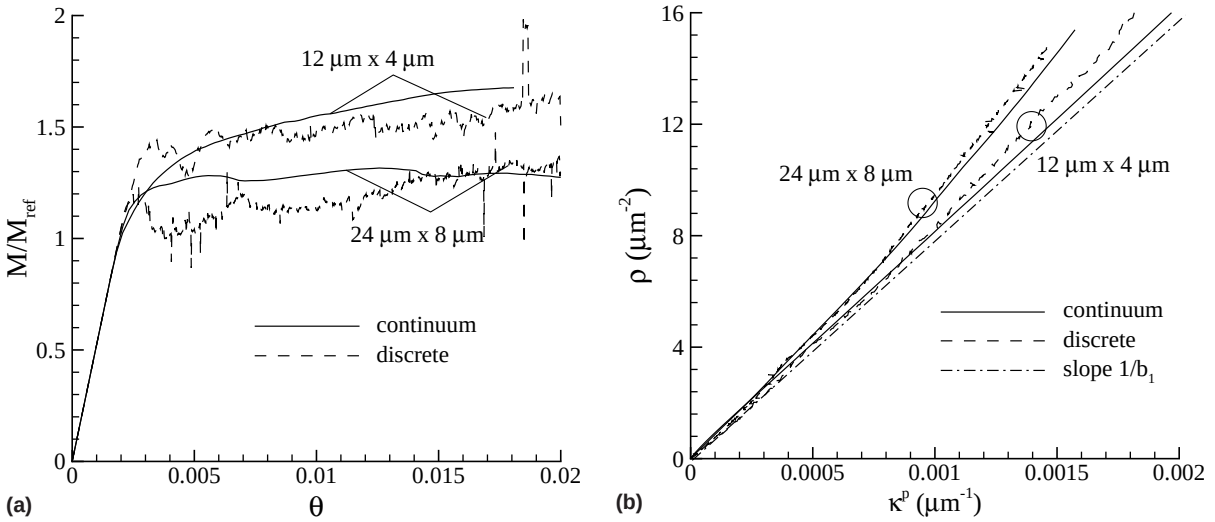

Fig. 17. Effect of specimen size for slip systems at (60°, 120°) on (a) the moment versus rotation angle and (b) total dislocation density evolution versus plastic curvature according to nonlocal continuum and discrete dislocation plasticity.

The results of the two calculations show that, due to the presence of the GNDs in the specimen, the response is size dependent and consistent with the conventional tendency of 'smaller being stronger'. A similar conclusion is obtained for slip systems at 60° and 120° as shown in Fig. 17. The two models predict also that the total dislocation density grows faster with plastic deformation for the bigger specimen and deviates from the linear asymptotic behaviour according to (35) (see Fig. 16b and Fig. 17b). However, in the bigger strip the deviation from the linear slope of the total density versus plastic curvature curve occurs at smaller plastic strains and is more prominent due to a larger population of statistical dislocations than for the reference size. In the continuum calculations, the dislocation density is generally somewhat lower with respect to the results of the discrete simulations, but the effect is picked up qualitatively well.

5. Conclusion

We have addressed the problem of extending the recently formulated nonlocal crystal plasticity theory for single slip (Yefimov et al., 2004a) to multiple slip in two dimensions. Continuum dislocation dynamics in multiple slip has been proposed based on the dynamics derived for single slip, and coupled to the small-strain framework of conventional continuum single crystal plasticity. Nonlocal interactions between the dislocations on different slip systems have been taken into account and the key issue of the form of these interactions has been addressed. Several possibilities to account for the orientation dependence of the nonlocal interactions have been considered on phenomenological grounds.

To investigate the capabilities of the theory in multiple slip, it has been applied to two boundary value problems. One problem is the simple shearing between two rigid and impenetrable walls of a single crystal oriented for symmetric double slip. Comparison of the results for different nonlocal interactions rules with discrete dislocation results of Shu et al. (2001) has singled-out the one that gives rise to negative off-diagonal elements of the projection matrix. The other interaction rules tend to overestimate the flow stress and shift the yield point upwards. Based on this comparison, the interaction law expressed in (22) and (23) is the best among those considered here. Numerous other phenomenological ones may be analyzed and a more

accurate interaction may be found, but within the present approach it seems more suited to await the rigorous statistical analysis of multiple slip along the lines of Zaiser et al. (2001).

The nonlocal plasticity calculations predict the formation of two distinct layers at the top and bottom surfaces of the strip, densely populated by the GNDs, much like the discrete simulations. The thickness of the boundary layers and the shape of the non-uniform shear strain profiles across the strip thickness are also in a good agreement with the results of the discrete dislocation plasticity simulations. The theory is also shown to be able to predict the size effect triggered by the presence of the boundary layers of GNDs, whose thickness does not scale with the strip height.

The other problem that has been addressed in this study concerns the bending of a single-crystal strip in plane strain with double slip. The nonlocal plasticity calculations have shown that, consistent with the discrete dislocation predictions of Cleveringa et al. (1999) for the same problem, the bending response for double slip shows significantly less hardening than in single slip. The presence of a significant population of statistically stored dislocations in the material, which originate, to large extent, from nonlocal interactions between different slip systems, has been also predicted. The orientation dependence of the bending response and the size effects for different slip orientations are consistent with the results of discrete dislocation simulation of the problem.

The present study for multiple slip, together with the previous ones (Yefimov et al., 2004a,b) for single slip, have shown that the proposed nonlocal continuum theory is able to handle various boundary value problems with different types of boundary conditions and to capture nonlocal effects. Contrary to phenomenological theories where strain gradients are added to the constitutive framework as internal variables (e.g., Fleck et al., 1994; Fleck and Hutchinson, 1997; Gao et al., 1999; Gurtin, 2002), nonlocality in the present theory arises from the dislocation dynamics. The length scale in this theory is not a constant, as in all phenomenological theories to date, but is controlled by the dislocation density which generally evolves with deformation. This series of the studies has also revealed that, once fitted to a particular boundary value problem, the theory is able to produce physically relevant solutions of other boundary value problems for the same material without any additional tuning. The variety of applications that the theory can handle is limited, however, by the two-dimensional nature of the theory.

Acknowledgment

This research was carried out under project number MS97006 in the framework of the Strategic Research Program of the Netherlands Institute for Metals Research in the Netherlands (www.nimr.nl).

References

Asaro, R.J., 1983. Micromechanics of crystals and polycrystals. Adv. Appl. Mech. 23, 1.

Ashby, M.F., 1970. The deformation of plastically non-homogeneous materials. Phil. Mag. 21, 399.

Bassani, J.L., Needleman, A., Van der Giessen, E., 2001. Plastic flow in a composite: a comparison of nonlocal continuum and discrete dislocation predictions. Int. J. Solids Struct. 38, 833–853.

Bittencourt, E., Needleman, A., Gurtin, M.E., Van der Giessen, E., 2003. A comparison of nonlocal continuum and discrete dislocation plasticity predictions. J. Mech. Phys. Solids 51, 281–310.

Cleveringa, H.H.M., Van der Giessen, E., Needleman, A., 1999. A discrete dislocation analysis of bending. Int. J. Plast. 15, 837–868.

Fleck, N.A., Hutchinson, J.W., 1997. Strain gradient plasticity. Adv. Appl. Mech. 33, 295–361.

Fleck, N.A., Muller, G.M., Ashby, F., Hutchinson, J.W., 1994. Strain gradient plasticity: theory and experiment. Acta Metall. Mater. 42, 475–487.

Gao, H., Huang, Y., Nix, W.D., Hutchinson, J.W., 1999. Mechanism-based strain gradient plasticity–I. Theory. J. Mech. Phys. Solids 47, 1239–1263.

Groma, I., 1997. Link between the microscopic and mesoscopic length-scale description of the collective behaviour of dislocations. Phys. Rev. B 56, 5807–5813.

Gurtin, M.E., 2002. A gradient theory of single-crystal viscoplasticity that accounts for geometrically necessary dislocations. J. Mech. Phys. Solids 50, 5–32.

Harder, J., 1999. A crystallographic model for the study of local deformation processes in polycrystals. Int. J. Plast. 15, 605–624.

Hutchinson, J.W., 2000. Plasticity at the micron scale. Int. J. Solids Struct. 37, 225–238.

Ma, Q., Clarke, D.R., 1995. Size dependent hardness of silver single crystals. J. Mater. Res. 10, 853–863.

Nye, J.F., 1953. Some geometrical relations in dislocated crystals. Acta. Metall. 1, 153–162.

Shu, J.Y., Fleck, N.A., 1999. Strain gradient crystal plasticity: size-dependent deformation of bicrystals. J. Mech. Phys. Solids 47, 297–324.

Shu, J.Y., Fleck, N.A., Van der Giessen, E., Needleman, A., 2001. Boundary layers in constrained plastic flow: Comparison of nonlocal and discrete dislocation plasticity. J. Mech. Phys. Solids 49, 1361–1395.

Stölken, J.S., Evans, A.G., 1998. A microbend test method for measuring the plasticity length scale. Acta Mater. 46, 5109–5115.

Van der Giessen, E., Needleman, A., 1995. Discrete dislocation plasticity: a simple planar model. Model. Simul. Mater. Sci. Eng. 3, 689–735.

Yefimov, S., Groma, I., Van der Giessen, E., 2004a. A comparison of a statistical-mechanics based plasticity model with discrete dislocation plasticity calculations. J. Mech. Phys. Solids 52, 279–300.

Yefimov, S., Groma, I., Van der Giessen, E., 2004b. Bending of a single crystal: discrete dislocation and nonlocal crystal plasticity simulations. Modelling Simul. Mater. Sci. Eng. 12, 1069–1086.

Zaiser, M., Carmen Miguel, M., Groma, I., 2001. Statistical dynamics of dislocation systems: the influence of dislocation–dislocation correlations. Phys. Rev. B 64, 224102–224111.